instruments

MDPI

Article

Attosecond Pulses from Ionization Injection Wakefield Accelerators

Paolo Tomassini [1,2,*], Vojtech Horny [1] and Domenico Doria [1]

[1] IFIN-HH ELI-NP, 077125 Magurele, Romania
[2] CNR-INO, 56124 Pisa, Italy
* Correspondence: paolo.tomassini@eli-np.ro

Abstract: High-quality ionization injection methods for wakefield acceleration driven by lasers or charged beams (LWFA/PWFA) can be optimized so as to generate high-brightness electron beams with tuneable duration in the attosecond range. We present a model of the minimum bunch duration obtainable with low-emittance ionization injection schemes by spotting the roles of the ionization pulse duration, of the wakefield longitudinal shape and of the delay of the ionization pulse position with respect to the node of the accelerating field. The model is tested for the resonant multi-pulse ionization injection (ReMPI) scheme, showing that bunches having a length of about 300 as can be obtained with an ionization pulse having a duration of 30 fs FWHM.

Keywords: attosecond electron bunches; ionization injection; two-color ionization injection; resonant multi-pulse ionization injection; trojan horse

check for updates

Citation: Tomassini, P.; Horny, V.; Doria, D. Attosecond Pulses from Ionization Injection Wakefield Accelerators. *Instruments* **2023**, *7*, 34. https://doi.org/10.3390/instruments7040034

Academic Editors: Alessandro Cianchi and Mario Galletti

Received: 12 September 2023
Revised: 10 October 2023
Accepted: 17 October 2023
Published: 24 October 2023

1. Introduction

The generation of relativistic electron bunches with durations in the attosecond range can lead to pump/probe beams, which can be fruitfully employed to unveil ultrafast dynamics [1]. In the context of plasma wakefield acceleration either driven by laser pulses (LWFA) [2] or particle beams (PWFA) [3], several methods have been proposed to specifically generate electron beams with a duration below the femtosecond scale, from the pioneering work about beam compression of beams externally injected ahead of the driver laser pulse [4–6], dense attosecond beams with up-ramp density transitions [7], attosecond beams via density modulations [8], attosecond trains obtained by betatron quivering modulations [9,10], few-cycle TW pulses-driven electron beams [11,12], attosecond trains via ionization injection [13] and high-brightness electron beams through ionization injection in hybrid LWFA/PWFA schemes [14,15]. As the disentanglement of the electron beam parameters including length, charge, average energy, energy spread and emittance are of paramount importance for the feasibility of the pump/probe attosecond source, thus a flexible injection/acceleration scheme should be preferred. The two-color ionization injection [16] and the resonant multi-pulse ionization injection (ReMPI) for LWFA [17], or their equivalent form for the PWFA, a.k.a. the trojan-horse scheme, result in being extremely flexible yet capable of generating high-brightness electron beams [15]. All these schemes use a driver to excite a large-amplitude plasma wave and a short-wavelength ionization pulse to extract electrons from a dopant. The driver can be a single long-wavelength laser pulse (two-color), a train of resonantly delayed pulses (ReMPI) or a charged beam (trojan horse). In any of these schemes, the electrons extracted by the low normalized amplitude ionization pulse ($a_{0,i} = eA_{0,i}/m_e c^2 \simeq 8.5 \times 10^{-10}\sqrt{I\lambda_i^2} \ll 1$, where I and λ_i are the ionization pulse peak intensity and wavelength in W/cm^2 and μm, respectively) do quiver in the laser field until they slip back out with a residual transverse momentum, which will constitute the major contribution for the final beam emittance. As the electrons are accelerated and focused by the wakefield, they are eventually trapped in the bucket and further accelerated.

During the slippage in the back of the bucket, the electron beam is compressed in both the longitudinal and radial directions and can reach longitudinal sizes of tens of nm, thus generating electron bunches that can reach attosecond-scale duration. As the wakefield driver should not ionize the dopant, its maximum electric field should be well below the threshold for tunnel ionization [18] of the selected ionization process (usually $He^{1^+\to 2^+}$, $Kr^{8^+\to 9^+}$, $Ar^{8^+\to 9^+}$) but its wakefield driving strength (which depends on the driver laser irradiance $I_d\lambda_d^2$ for LWFA schemes or on the driver beam electric field for PWFA) should be large enough to be able to excite wakefields with amplitudes above the trapping threshold for the extracted electron beam [19]. These contradictory requests have been solved in the two-color [16] scheme by employing a single driver pulse having a long wavelength (so as to increase the irradiance while keeping the pulse electric field below the dopant ionization threshold), thus raising the request for using two-laser systems. The ReMPI scheme [17] can also use a single-laser system (e.g., a Ti:Sa one), and it employs a train of resonantly delayed pulses, each one having an electric field below the ionization threshold. The particle-driven-based ionization injection scheme [15] is in a particularly favorable position here, as in both the laser and particle driven cases, the wakefield amplitude should exceed the trapping threshold, but the electric field associated with the particle driver is much lower than that related to the laser-driven option. This opens the possibility of employing ionization processes with low ionization thresholds as $He^{1^+\to 2^+}$, thus paving the road for ultralow-emittance electron beams.

2. Materials and Methods

In the following, we will consider the dynamics of electrons extracted by a field (tunnel) ionization and immersed into a plasma wakefield driven by ultrarelativistic laser pulses or dense charged beams. The timescale T_{evol} of the driver evolution and of the background (eventual) plasma longitudinal variation will be much longer than the time $T_{charging}$ needed by the electron beam to be extracted and trapped by the wakefield, thus enabling us to employ the quasi-static approximation (QSA) [20]. When the particle dynamics are described in a moving window with the same speed v_d of the driver (say, along the z direction), the constant of motion [5]

$$\gamma(t) - \beta_d u_z - \phi(\xi(t), k_p\vec{x}_\perp(t)) \equiv h_0 = constant \tag{1}$$

unveils the longitudinal electron dynamics. In Equation (1), γ is the particle Lorentz factor, $\beta_d = v_d/c$, $\vec{u} = \vec{p}/m_e c$ and $\phi \equiv e\Phi/m_e c^2$ is the normalized scalar potential, $k_p = 2\pi/\lambda_p$ is the plasma wave wavevector and $\xi = k_p(z - v_d t)$ is the longitudinal coordinate inside the window. As any particle extracted by field ionization with very low pulse amplitude is ejected from the parent ion with a negligible momentum (it will obtain quivering and drift momentum in the laser field right after the ejection), we can easily evaluate the h_0 constant from Equation (1) as $h_0 = 1 - 0 - \phi_e$, where $\phi(\xi(t = t_e), k_p\vec{x}_\perp(t = t_e))$ is the normalized potential in the particles' position at the extraction time t_e. Right after the ejection from the ion, the electron quivers in the laser field, experiencing longitudinal and transverse ponderomotive forces as well as the longitudinal and transverse forces from the wakefield. In the window co-moving with the wakefield driver, the electron is seen slipping back towards the rear of the bucket and eventually being trapped by the wakefield. During the slippage, the electron beam is constituted by electrons extracted in different longitudinal positions in the co-moving window. As the Lorentz factor of the electrons increases during their slippage in the back of the bucket, the velocities of the particles approach the speed of light, and therefore the electron bunch becomes stiff along the longitudinal direction. The beam compression therefore occurs during the early stages of the beam acceleration and reaches its stable point around the turning point of the longitudinal trajectory in the co-moving window [5], i.e., at the particle trapping point, where the longitudinal speed

of the particles is the same as the wakefield, i.e., that of the driver. After straightforward manipulations of Equation (1) at the trapping point occurring at t_t, we obtain

$$\frac{\gamma_{\perp,t}}{\gamma_d} - \phi_t = 1 - \phi_e \ , \tag{2}$$

where $\phi_t = \phi(\xi(t = t_t), k_p \vec{x}_\perp(t = t_t))$ is the normalized potential at the trapping point and $\gamma_{\perp,t} = \sqrt{1 + u_\perp^2(t = t_t)}$ is the transverse Lorentz factor at the trapping time. Equation (2) states that at the trapping point, the normalized potential where the particle is placed (ϕ_t) depends only on the potential where the particle was born (ϕ_e) and on the transverse momentum of the particle (through $\gamma_{\perp,t}$) at the trapping time. This link constitutes the basis for the evaluation of the beam length, which will depend on wakefield parameters and on the spread of the longitudinal and transverse position of the particles at their extraction time. We can accurately estimate this spread, as well as the rms residual transverse momentum, by using the theory in [21]. Here, we limit ourselves to the unsaturated ionization regime in the tunnel regime and to leading order in the parameter [22] $\Delta = \left(\frac{3E_0}{2E_a}\right)^{1/2}\left(\frac{U_H}{U_I}\right)^{1/2} \approx 0.2$, where E_0 is the ionization pulse peak electric field, $E_a \simeq 0.51$ TV/m is the atomic field, U_I is the ionization energy of the ionization process and $U_H = 13.6$ eV is the ionization energy of the hydrogen atom. Theory in [21,22] shows that for a laser pulse of minimum waist $w_{0,i}$, normalized amplitude $a_{0,i}$ and FWHM duration T_i, the rms residual transverse momentum ($u_{\perp,e}$), radius (r_e) and length (δz_e) of the beam can be evaluated as

$$\sigma(u_{\perp,e}) \simeq \Delta a_{0,i}, \ \ \sigma(r_e) \simeq \Delta w_{0,i}, \ \ \sigma(\delta z_e) \simeq \frac{1}{\sqrt{2}} \Delta L_{0,i}, \tag{3}$$

where $L_{0,i} = cT_i/\sqrt{2\log 2}$. Details of electrons extraction and rms residual transverse momentum for the ReMPI simulations reported here can be found in Figure 1.

In what follows, we will also neglect the slippage of the ionization pulse in the wakefield structure. The distance of the ionization pulse from the wakefield driver can either increase or decrease, depending upon the employed scheme, but its variation is usually negligible, as the ionization pulse is tightly focused. The particle extraction process lasts for a time $T_{charging} \approx Z_r/c = \pi w_{0,i}^2/\lambda_i c$, and in this time interval, the change in longitudinal position of the pulse envelope with respect to the wakefield is $\delta z_{envelope} \simeq T_{charging}(v_i - v_d)$, where $v_i \simeq c[1 - n_e/2n_c(\lambda_i)]$ is the ionization pulse speed, n_e is the plasma density and $n_c(\lambda_i) = 1.1 \times 10^{21}/\lambda_i^2$ is the critical density for the ionization pulse. For two-color and ReMPI schemes, the driver is a laser pulse with wavelength λ_d longer than that of the ionization pulse. For those schemes, the ionization pulse moves towards the driver a distance of $\delta z_{envelope} \simeq Z_r n_e[(\lambda_d/\lambda_i)^2 - 1]/2n_c(\lambda_i)$, while for a particle-driven wakefield, the pulse moves back a distance of $\delta z_{envelope} \simeq \frac{1}{2} Z_r[n_e/n_c(\lambda_i) - 1/\gamma_d^2]$. The final effect of pulse slippage will be negligible provided that $L_i \ll Z_r/c|(v_i - v_d)|$. For the case of an ReMPI scheme driven by a Ti:Sa pulse with plasma density of $n_e = 10^{18}$ cm^{-3} and ionization pulse with $w_{0,i} = 4.5$ µm, $L_i = 10$ µm, $\lambda_i = \lambda_d/3$, we obtain $\delta z_{envelope} \simeq 0.06$ µm. With a two-color setup in a plasma driven by a $\lambda_d = 5$ µm pulse propagating into a plasma having density $n_e = 10^{17}$ cm^{-3} and with an ionization pulse having $w_{0,i} = 4.5$ µm, $L_i = 10$ µm, $\lambda_i = 0.4$ µm, we obtain $\delta z_{envelope} \simeq 0.3$ µm. In both the ReMPI and two-color cases, the ionization pulse slippage is much smaller than L_i. Due to the very large Lorentz factor of the driver beam for the PWFA case, the ionization pulse slippage for the trojan-horse injector is even smaller than that for the laser-driven schemes.

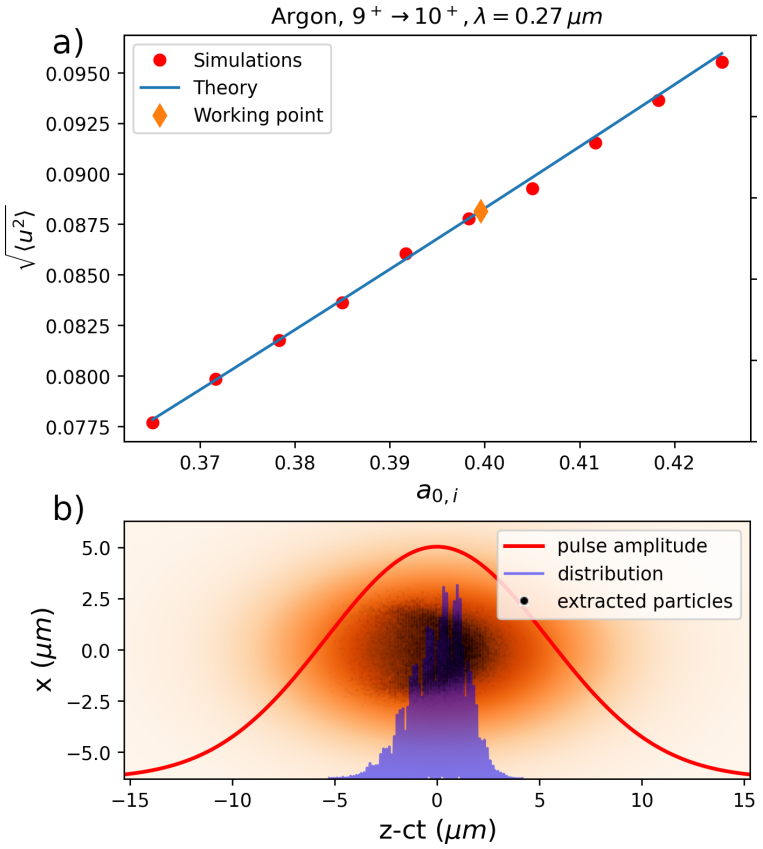

Figure 1. Extraction of the electrons by the tunnel ionization process in the ionization pulse field. (**a**) Scan of the residual transverse momentum in the laser polarization axis versus the ionization pulse peak amplitude $a_{0,i}$. Results from simulations (red dots) are in full agreement with the theory in [21] for the $Ar^{9^+ \to 10^+}$ process, as the available Ar^{8^+} electrons were already extracted by the driving train. (**b**) Ionization pulse field envelope and extracted electrons' positions. The resulting longitudinal and transverse extension of the extracted bunch $\sigma(\delta z_e = z_e - ct_e) \simeq 1.33$ μm and $\sigma(x_e) \simeq 1.11$ μm are in agreement with predictions in [21,22].

The wakefield structure can be obtained from analytical results in the blowout regime [23] and by PIC (or fluid simulation if no wave breaking occurs). We performed quasi-3D simulations for the ReMPI scheme in the quasi-linear regime by means of the FB-PIC code [24]. There, a 4.5 J Ti:Sa pulse is split into two sub-pulses after a pick-up of a 100's mJ small-size beam for the frequency tripled ionization injection. The driving train of two resonantly delayed and circularly polarized pulses had a duration of 23 fs, waist of 30 μm and normalized amplitude of $a_{0,d} = 0.9$, while the linearly polarized ionizing pulse had a FWHM duration of $T_i = 30$ fs, waist of $w_{0,i} = 4.2$ μm and amplitude of $a_{0,i} = 0.4$. The ionization pulse phase position in the bucket was varied in the interval $-0.7 \leq \bar{\xi}_e \leq 0.7$. A plasma target composed by argon (pre-ionized up to the 8th level) with an electron density of $n_e = 7.5 \times 10^{17}$ cm^{-3}, corresponding to a plasma wave vector of $k_p = 0.164$ μm^{-1}, is considered. The driver Lorentz factor was $\gamma_d = \sqrt{n_c/n_e} \simeq 48$, where $n_c = 1.1 \times 10^{21}/\lambda_d^2 = 1.7 \times 10^{21}$ cm^{-3} is the critical density for the driver with wavelength $\lambda_d = 0.81$ μm. The beam extraction process lasted for a time $T_{charging} \approx 900$ fs, corresponding to an ionization pulse propagation of about one Rayleigh length. The electron beams, having a charge of $Q = 5.2$ pC and normalized emittance of about 80 nm rad in the ionization pulse polarization axis, were analyzed in a simulation time at which the trapping was completed. The fields in the simulated cylindrical region were sampled with $N_m = 3$ rotational modes, and $2 \times 2 \times 12 = 48$ particles per cell were deposited in the r, z, θ directions of the cell. The spatio-temporal resolution was $dz = \lambda_i/24$ and $dr = \lambda_i/8$ in the longitudinal and radial directions, with $\lambda_i = \lambda_d/3 \simeq 270$ nm being the ionization pulse wavelength. A snapshot of

the fields for the case $T_i = 30$ fs is shown in Figure 2. Those simulations (see Figure 2) show that the longitudinal field on the axis exhibits a linear shape within the whole ionization pulse, with slope $\partial_{\bar{\xi}} \hat{E}_z^e = 0.38$. For the simulation shown there, the average field at the extraction is $\hat{E}_z^e = -0.3$ and the resulting average electric field at trapping is $\hat{E}_z^e = -0.72$, which agrees with the one inferred by asking if the particles are trapped close to the peak of the accelerating gradient [17]. We stress here that the slight positive or negative delay of the ionization pulse with respect to the field node resulting in $|\bar{\xi}_e| \lesssim 1$ will barely change the electric field at trapping. The radial structure of the electric field also exhibits, as expected, a linear shape close to the axis with gradient $\partial_{k_p r_e} \hat{E}_r^e = 0.04$, which is much smaller than that obtainable in the blowout regime (1/4 [23]).

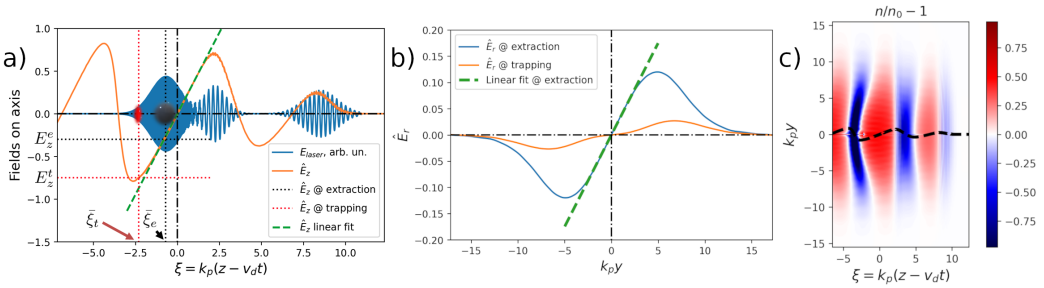

Figure 2. Field structure for one of the ReMPI simulations in the quasi-linear regime and for a case in which the ionization pulse is delayed from its optimal position in $\bar{\xi} = \bar{\xi}_e = 0$. (**a**) Line-out on the axis: the accelerating field (orange) is in units of E_0, the laser pulses transverse field (blue) is in arbitrary units. The ionization pulse is placed in the phase $\bar{\xi}_e = -0.7$, with an average longitudinal field at extraction $\hat{E}_z^e = -0.3$. The longitudinal field at trapping ($\bar{\xi}_t = -2.3$) is $\hat{E}_z^e = -0.72$. The dashed (green) line shows a linear fit of the accelerating gradient at $\bar{\xi} = 0$. (**b**) Transverse line-out of the transverse field normalized to E_0 in the node of the longitudinal field (blue) and on the trapping point (orange). The dashed (green) line shows a linear fit of the transverse gradient at $\bar{\xi} = 0$. (**c**) 2D map of $n(\bar{\xi}, k_p r)/n_e - 1$ showing that a quasi-linear regime is obtained. The dashed line represents the accelerating gradient in arb. units.

3. Results

In the following, we will suppose the ionization pulse size is much smaller than that of the wakefield, i.e., $cT_i \ll \lambda_p$, and $w_{0,i} \ll R$, where T_i and $w_{0,i}$ are the FWHM pulse duration and minimum waist and R is the wakefield radius. These assumptions will assure us that all the extracted electrons will lie in a similar potential at the extraction time. The constraint $w_{0,i} \ll R$, along with the constraint $a_{0,i} \ll 1$, will also limit the extent of the transverse dynamics of the extracted electrons, thus maintaining the normalized transverse momentum in the non-relativistic range $|\vec{u}_{\perp,t}| \ll 1$. Simulations with the ReMPI scheme show that at the trapping point, the bunch transverse size is a fraction of a μm (and usually smaller than the transverse size at the extraction time), while the transverse momentum is close to the one right after the ionization pulse passage. We will also consider non-evolving wakefields in the temporal window of the electrons extraction and trapping process, so as to ensure that the potential function $\phi(\bar{\xi}, k_p \vec{r})$ is a constant of time. This will limit the amount of the charge for the trapped beam down to the pC level, as beam-loading effects might change the wakefield around the trapped beam position.

For a wakefield with rotational symmetry, the second-order Taylor expansion of the normalized potential close to the axis turns out to be

$$\phi(\bar{\xi}_0 + \delta\bar{\xi}, k_p r) \simeq \phi(\bar{\xi}_0, 0) - \hat{E}_z(\bar{\xi}_0, 0)\delta\bar{\xi} - \frac{1}{2}\left(\partial_{\bar{\xi}} \hat{E}_z(\bar{\xi}, 0)|_{\bar{\xi}_0} \delta\bar{\xi}^2 + \partial_{k_p r} \hat{E}_r(\bar{\xi}_0, k_p r)|_0 (k_p r)^2\right), \quad (4)$$

where $\hat{E}_{z,r} = -\partial_{\bar{\xi}, k_p r}\phi = E_{z,r}/E_0$ are the longitudinal and radial electric field components normalized to the Dawson field $E_0 = mc^2 k_p / e$.

We can now consider a set of electrons emitted by field ionization at slightly different longitudinal and transverse positions $(\xi_e, k_p r_e)$, which will result in the trapping point being in the position $(\xi_t, k_p r_t)$. The center of mass (phase) position of the beam at the extraction time is $(\bar{\xi}_e, 0)$ (where $\bar{\xi}_e \equiv \langle \xi_e \rangle$), which lies in the potential $\bar{\phi}_e = \phi(\bar{\xi}_e, 0)$. By implicitly defining the *reference* position $(\bar{\xi}_t, 0)$ of the beam at its trapping point through the relation Equation (2)

$$\bar{\gamma}_{\perp,t}/\gamma_d - \bar{\phi}_t = 1 - \bar{\phi}_e, \tag{5}$$

where $\bar{\phi}_t = \phi(\bar{\xi}_t, 0)$ and $\bar{\gamma}_{\perp,t} = \langle \gamma_{\perp,t} \rangle$, we can access the information of the longitudinal spread of the particle position by inverting the nonlinear equation

$$\frac{\gamma_{\perp,t}}{\gamma_d} - \phi(\bar{\xi}_t + \delta\xi_t, k_p r_t) = 1 - \phi(\bar{\xi}_e + \delta\xi_e, k_p r_e) \tag{6}$$

on the variable $\delta\xi_t$. As we seek ultrashort pulses of length $\delta z_t \simeq \sigma(\delta\xi_t)/k_p \ll 1$ (here $\sigma(x)$ is the rms value of the random variable x), at the trapping point, the longitudinal gradient of the normalized potential should dominate over the radial one. As a result, particles should be trapped where the accelerating gradient is as high as possible. This is accomplished by setting the wakefield amplitude and the extraction position so that the strong trapping condition is reached [17]. As the radial contribution of the normalized potential ϕ spread at the trapping point is negligible over the longitudinal one, we can express Equation (7) by using the expansion in Equations (2) and (4) to obtain

$$\frac{\delta\gamma_{\perp,t}}{\gamma_d} + \hat{E}_z^t \delta\xi_t \simeq \hat{E}_z^e \delta\xi_e + \frac{1}{2}\left(\partial_{\xi}\hat{E}_z^e \delta\xi_e^2 + \partial_{k_p r_e}\hat{E}_r^e (k_p r_e)^2\right), \tag{7}$$

where $\hat{E}_z^t = \hat{E}_z(\bar{\xi}_t, 0)$, $\hat{E}_z^e = \hat{E}_z(\bar{\xi}_e, 0)$, $\partial_{\xi}\hat{E}_z^e = \partial_{\xi}\hat{E}_z(\xi, 0)|_{\xi_e}$, $\partial_{k_p r_e}\hat{E}_r^e = \partial_{k_p r_e}\hat{E}_r(\xi_e, k_p r)|_0$ and $\delta\gamma_{\perp,t} = \gamma_{\perp,t} - \bar{\gamma}_{\perp,t} \simeq \frac{1}{2}(u_\perp^2 - \langle u_\perp^2 \rangle)$, which is valid for $u_\perp^2 \ll 1$. The average longitudinal field at extraction ($\hat{E}_z^e$), trapping ($\hat{E}_z^t$) and field slopes at extraction ($\partial_{\xi}\hat{E}_z^e$, $\partial_{k_p r_e}\hat{E}_r^e$) depend on the phase of the ionization pulse within the bucket and on the wakefield's regime. They can be analytically inferred in the blowout regime [23] or obtained by simulations. Typical values of $\partial_{\xi}\hat{E}_z^e$ and $\partial_{k_p r_e}\hat{E}_r^e$ for the quasi-linear regime at the threshold for the strong trapping or the blowout regimes can be found in Table 1 (see also Figure 2). We refer there to quasi-3D simulations we performed for an ReMPI setup in the quasi-linear regime (at least during the beam charging/trapping time). Those simulations will be discussed in detail below.

Table 1. Longitudinal and radial gradients of the electric field at the node of the longitudinal electric field (see Figure 2).

Parameter	Quasi-Linear	Spherical Bubble (Theory)
$\partial_{\xi}\hat{E}_z^e$	0.38	0.50
$\partial_{k_p r_e}\hat{E}_r^e$	0.04	0.25

To simplify Equation (7), we employ the linearity of the longitudinal field in the vicinity of the node (where the ionization pulse is placed), thus substituting the average field $\hat{E}_z^e$ at the extraction with $\hat{E}_z^e \simeq \partial_{\xi}\hat{E}_z^e \cdot \bar{\xi}_e$ for $|\bar{\xi}_e| \lesssim 1$:

$$\hat{E}_z^t \delta\xi_t \simeq \partial_{\xi}\hat{E}_z^e \left(\bar{\xi}_e \delta\xi_e + \frac{1}{2}\delta\xi_e^2\right) + \frac{1}{2}\partial_{k_p r_e}\hat{E}_r^e (k_p r_e)^2 - \frac{\delta\gamma_{\perp,t}}{\gamma_d}. \tag{8}$$

Let us first evaluate the average of the phase positions spread at trapping $\bar{\xi}_t = \langle \xi_t \rangle$ by averaging Equation (8) on the random variables $\delta\xi_e$ and r_r, which are independently distributed

$$\hat{E}_z^t \langle \delta\xi_t \rangle \simeq \frac{1}{2}\left(\partial_{\xi}\hat{E}_z^e \sigma^2(\xi_e) + \partial_{k_p r_e}\hat{E}_r^e k_p^2 \sigma^2(r_e)\right). \tag{9}$$

We aim at evaluating the variance of $\delta\xi_t$, so we need to average the square of the right-hand side of Equation (8). This involves terms a $\langle\delta\gamma_{\perp,t}^2\rangle/\gamma_d^2 \approx \frac{1}{4}\sigma^2(u_\perp)/\gamma_d^2 \approx \frac{3}{4}\Delta^2 a_{0,i}^2/\gamma_d^2$, which can be neglected, as $\gamma_d \gg 1$, $a_{0,i}^2 \ll 1$ and $\Delta^2 = \mathcal{O}(10^{-3})$. In the following, we will assume γ_d to be sufficiently large to neglect all the terms containing $\delta\gamma_\perp^2/\gamma_d^2$. The evaluation of the $\delta\xi_t$ variance $\sigma^2(\delta\xi_t^2) = \langle\delta\xi_t^2\rangle - \langle\delta\xi_r\rangle^2$ finally leads to:

$$2(\hat{E}_z^t)^2\sigma^2(\delta\xi_t) \simeq (\partial_{\bar{\xi}}\hat{E}_z^e)^2\left[2\bar{\xi}_e^2\sigma^2(\delta\xi_e) + \sigma^4(\delta\xi_e)\right] + (\partial_{k_p r_e}\hat{E}_r^e)^2 k_p^4\sigma^4(r_e)\,. \tag{10}$$

We can immediately see from Equation (10) that if all the wakefield parameters and all the ionization pulse parameters (but the ionization pulse phase $\bar{\xi}_e$) are fixed, the rms value of the longitudinal positions at trapping $\sigma(z_t)$ obtains its minimum value when the ionization pulse is placed in the vicinity of the node (where $\bar{\xi}_e = k_p\bar{z}_e \approx 0$). This was expected, as in the neighbors of the node of the longitudinal gradient, the scalar potential is symmetric, which leads to similar trapping positions for particles extracted at phases ξ_e and $-\xi_e$, provided that $|\xi_e| \ll 1$.

We evaluate the terms of Equation (10) for the reference case given by the ReMPI simulations we run and for the case of the fully evacuated bubble. For the blowout case, we will use the analytical results from [23] and we will assume that both a background plasma and an ionization pulse with the same parameters as the ReMPI PIC simulations will be employed. We also evaluate the neglected term related to $\delta\gamma_\perp^t/\gamma_d$ to check the accuracy of the approximation we made.

Results are shown in Table 2, where it is apparent that the transverse contributions are much smaller than the longitudinal ones in the case of tightly focused ionization pulses ($cT_i \gg w_{0,i}$). In addition, the terms related to the transverse momentum spread at the trapping point are negligible for the cases considered above. The rms longitudinal beam size at trapping can be directly expressed in terms of physical quantities as

$$\sigma(\delta z_f) \simeq k_p\Delta^2\sqrt{\frac{1}{2E_z^t}\left\{(\partial_{\bar{\xi}}\hat{E}_z^e)^2\left[\frac{1}{4} + \left(\frac{\bar{z}_e}{\Delta L_i}\right)^2\right]L_i^4 + (\partial_{k_p r_e}\hat{E}_r^e)^2 w_{0,i}^4\right\}}, \tag{11}$$

where $\bar{z}_e$ is the position of the ionization pulse with respect to the node of the electric field (where we set $\xi = 0$ in Figure 2). Equation (11) gives us the route to obtain ultrashort electron beams. Firstly, as stated above, the electric field at the trapping point should be as large as possible. If a quasi-linear regime is employed, the strong trapping condition [17] assures that the electron beam is trapped at the peak of the electric field. Secondly, as the beam length scales as $k_p \propto n_e^{-1/2}$, tenuous plasmas might be preferred also because they led to higher values for γ_d in the case of a laser driver. Finally, as the term $\bar{z}_e/(\Delta Li)$ in Equation (11) refers to the ratio between the distance of the ionization pulse to the node ($\bar{z}_e$) and the longitudinal extension of the beam at the extraction time ($\Delta L_i/\sqrt{2}$), we can obtain the shortest electron beams by placing the ionization pulse on the node of the accelerating gradient, with an acceptable jitter of the scale of a fraction of the ionization pulse length, i.e., $|\bar{z}_e| \ll (\Delta L_i)$. Results for dependence of the rms beam duration $\sigma(\delta t_e) = \sigma(\delta z_e)/c$ on the delay of the ionization pulse from the accelerating gradient node $\bar{z}_e/c$ are shown for the case of the ReMPI setup with a 200 TW Ti:Sa laser system selected here and with $T = 30$ fs long ionization pulse in third harmonics. Predictions from the model (Equation (11)) do overlap with the observed beam duration, which shows that electron beams with duration as short as 300 as can be generated in this way (see Figure 3). As both the ionization pulse and the driver train are generated by the same amplified pulse, the relative time jitter between them is only due to mechanical vibration of the optical elements after the pick-up, and it can therefore be limited down to a few femtoseconds scale.

Table 2. Estimation of the terms in Equation (10).

Parameter	Quasi-Linear	Spherical Bubble (Theory)
$[\partial_{\tilde{\xi}} \hat{E}_z^e \sigma(\delta\xi_e)^2]^2$	3×10^{-4}	4×10^{-4}
$[\partial_{k_p r_e} \hat{E}_r^e k_p^2 \sigma(r_e)^2]^2$	1×10^{-6}	5×10^{-5}
$[\sigma(\delta\gamma_\perp^t)/\gamma_d]^2$	4×10^{-8}	4×10^{-8}

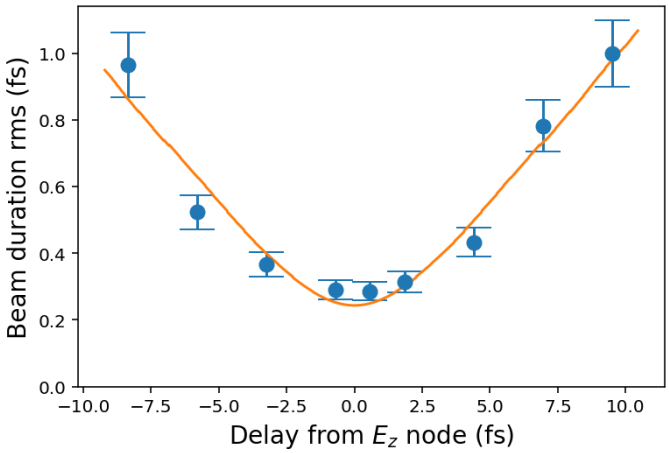

Figure 3. Beam duration rms at the trapping point for the set of ReMPI simulations with ionization pulse duration of 30 fs FWHM vs. the delay $\bar{z}_e/c$ of the ionization pulse with respect to the node of the electric field. The error bars were estimated by considering the discrepancy between the rms values obtained with three distinct methods, i.e., direct evaluation of the variance from the particles positions, Gaussian fit and equivalent rms from median absolute deviation robust analysis. The central point was obtained by averaging the three outcomes, and the error bars are the dispersion values. The orange line refers to the prediction by Equation (11) for the ReMPI simulation reported in Section 2 and with the wakefield parameters in Table 1.

4. Discussion

We discussed here a simple model to infer the beam duration of electron beams obtained by high-quality ionization injection schemes (e.g., two-color, ReMPI or trojan horse) with an ultrarelativistic wakefield driver ($\gamma_d \gg 1$), low amplitude ($a_{0,i} \ll 1$) and tightly focused ($w_{0,i} \ll R$) and short ($k_p cT \ll 1/\Delta$) ionization pulses. Those conditions are naturally satisfied with the trojan-horse scheme, which employs electron beams with $\langle\gamma\rangle = \gamma_d \gg 1$ as drivers. As the ReMPI scheme can work with Ti:Sa pulses, at plasma densities in the range of $(1 \times 10^{17} - 1 \times 10^{18})$ cm^{-3}, the driver relativistic factor $\gamma_d = \sqrt{n_c/n_e}$ is in the range 40–130. The two-color scheme needs a long-wavelength driver ($\lambda_d = 5$ µm in [16]), so the achievement of the condition $\gamma_d \gg 1$ requires much lower plasma densities (a factor of five less to obtain the same γ_d with a Ti:Sa pulse). The model was tested against a set of ReMPI simulations in the quasi-linear regime, with $\gamma_d \simeq 50$. Both the minimum value of the beam duration (about 300 as rms) and the dependence of duration on the delay of the ionization pulse from the accelerating gradient node agree with a percent error. The model does not take into account beam loading effects, curvature effects of the $\xi - u_z$ trajectories at the inversion point (which decrease by employing high values of γ_d) and the eventual evolution of the wakefield during the beam charging, which can be caused by driver evolution or non-flat longitudinal background plasma profiles. The first effect can be mitigated by reducing the amount of the extracted charge, the second is virtually negligible in beam-driven schemes and it can be mitigated in laser-driven schemes by reducing the plasma density. The third one is negligible in trojan-horse-like schemes with flat plasma profiles, while it can be reduced in LWFA by choosing very small waist sizes for the ionization injection pulse and/or driver pulses close to their foci. The effect of the

ionization pulse-to-driver temporal jitter was also discussed. For an ReMPI scheme driven by a single Ti:Sa pulse, the time jitter of the ionization pulse to the node of the accelerating gradient can be limited down to a few femtoseconds, resulting in a slight increase in the trapped beam length for the case of ionization pulses of duration $T = 30$ fs FWHM. A similar scenario can be envisaged in trojan-horse schemes for which the photocathode laser pulse and the ionization pulse can be obtained from the same laser system.

Author Contributions: Conceptualization, P.T.; methodology, P.T.; software, P.T. and V.H.; validation, P.T. and V.H.; formal analysis, P.T. and V.H.; investigation, P.T., D.D. and V.H.; resources, D.D., V.H. and P.T.; data curation, P.T.; writing—original draft preparation, P.T.; writing—review and editing, P.T., D.D. and V.H.; visualization, P.T.; supervision, P.T.; project administration, D.D.; funding acquisition, D.D. and P.T. All authors have read and agreed to the published version of the manuscript.

Funding: Extreme Light Infrastructure Nuclear Physics (ELI-NP) Phase II is a project co-financed by the Romanian Government and the European Union through the European Regional Development Fund and the Competitiveness Operational Programme (1/07.07.2016, COP, ID 1334). This work was supported by the contract sponsored by the Romanian Ministry of Research and Innovation: PN 23 21 01 05 and the IOSIN funds for research infrastructures of national interest.

Data Availability Statement: Data are available upon reasonable request to the authors.

Acknowledgments: Access to HPC through PRACE EHPC-BEN-2023B05-023 is warmly acknowledged.

Conflicts of Interest: The authors declare no conflict of interest.

References

1. Krausz, F.; Ivanov, M. Attosecond physics. *Rev. Mod. Phys.* **2009**, *81*, 163–234. [CrossRef]
2. Tajima, T.; Dawson, J.M. Laser Electron Accelerator. *Phys. Rev. Lett.* **1979**, *43*, 267–270. [CrossRef]
3. Chen, P.; Dawson, J.M.; Huff, R.W.; Katsouleas, T. Acceleration of electrons by the interaction of a bunched electron beam with a plasma. *Phys. Rev. Lett.* **1985**, *54*, 693–696. [CrossRef] [PubMed]
4. Khachatryan, A.G. Trapping, compression, and acceleration of an electron beam by the laser wake wave. *J. Exp. Theor. Phys. Lett.* **2001**, *74*, 371–374. [CrossRef]
5. Khachatryan, A.G. Trapping, compression, and acceleration of an electron bunch in the nonlinear laser wakefield. *Phys. Rev. E* **2002**, *65*, 046504. [CrossRef]
6. Khachatryan, A.; Van Goor, F.; Boller, K.J.; Reitsma, A.; Jaroszynski, D. Extremely short relativistic-electron-bunch generation in the laser wakefield via novel bunch injection scheme. *Phys. Rev. Spec. Top. Accel. Beams* **2004**, *7*, 121301. [CrossRef]
7. Li, F.; Sheng, Z.; Liu, Y.; Meyer-ter Vehn, J.; Mori, W.; Lu, W.; Zhang, J. Dense attosecond electron sheets from laser wakefields using an up-ramp density transition. *Phys. Rev. Lett.* **2013**, *110*, 135002. [CrossRef]
8. Tooley, M.; Ersfeld, B.; Yoffe, S.; Noble, A.; Brunetti, E.; Sheng, Z.; Islam, M.; Jaroszynski, D. Towards attosecond high-energy electron bunches: Controlling self-injection in laser-wakefield accelerators through plasma-density modulation. *Phys. Rev. Lett.* **2017**, *119*, 044801. [CrossRef]
9. Luttikhof, M.; Khachatryan, A.; Van Goor, F.; Boller, K.J. Generating ultrarelativistic attosecond electron bunches with laser wakefield accelerators. *Phys. Rev. Lett.* **2010**, *105*, 124801. [CrossRef]
10. Horný, V.; Krůs, M.; Yan, W.; Fülöp, T. Attosecond betatron radiation pulse train. *Sci. Rep.* **2020**, *10*, 15074. [CrossRef]
11. Zhu, X.L.; Liu, W.Y.; Chen, M.; Weng, S.M.; He, F.; Assmann, R.; Sheng, Z.M.; Zhang, J. Generation of 100-MeV attosecond electron bunches with terawatt few-cycle laser pulses. *Phys. Rev. Appl.* **2021**, *15*, 044039. [CrossRef]
12. Ferri, J.; Horný, V.; Fülöp, T. Generation of attosecond electron bunches and x-ray pulses from few-cycle femtosecond laser pulses. *Plasma Phys. Control. Fusion* **2021**, *63*, 045019. [CrossRef]
13. Deng, A.; Li, X.; Luo, Z.; Li, Y.; Zeng, J. Generation of attosecond micro bunched beam using ionization injection in laser wakefield acceleration. *Opt. Express* **2023**, *31*, 19958–19967. [CrossRef] [PubMed]
14. Hidding, B.; Rosenzweig, J.; Xi, Y.; O'Shea, B.; Andonian, G.; Schiller, D.; Barber, S.; Williams, O.; Pretzler, G.; Königstein, T.; et al. Beyond injection: Trojan horse underdense photocathode plasma wakefield acceleration. *AIP Conf. Proc.* **2012**, *1507*, 570–575.
15. Hidding, B.; Assmann, R.; Bussmann, M.; Campbell, D.; Chang, Y.Y.; Corde, S.; Cabadağ, J.C.; Debus, A.; Döpp, A.; Gilljohann, M.; et al. Progress in hybrid plasma wakefield acceleration. *Photonics* **2023**, *10*, 99. [CrossRef]
16. Yu, L.L.; Esarey, E.; Schroeder, C.B.; Vay, J.L.; Benedetti, C.; Geddes, C.G.R.; Chen, M.; Leemans, W.P. Two-Color Laser-Ionization Injection. *Phys. Rev. Lett.* **2014**, *112*, 125001. [CrossRef]
17. Tomassini, P.; De Nicola, S.; Labate, L.; Londrillo, P.; Fedele, R.; Terzani, D.; Gizzi, L.A. The resonant multi-pulse ionization injection. *Phys. Plasmas* **2017**, *24*, 103120. [CrossRef]

18. Ammosov, M.V.; Delone, N.B.; Krainov, V.P. Tunnel Ionization of Complex Atoms and Atomic Ions in Electromagnetic Field. In Proceedings of the High Intensity Laser Processes: 1986 Quebec Symposium, Quebec City, QC, Canada, 3–6 June 1986; Alcock, J.A., Ed.; International Society for Optics and Photonics (SPIE): Bellingham, WA, USA, 1986; Volume 0664, pp. 138–141. [CrossRef]
19. Esarey, E.; Pilloff, M. Trapping and acceleration in nonlinear plasma waves. *Phys. Plasmas* **1995**, *2*, 1432–1436. [CrossRef]
20. Sprangle, P.; Esarey, E.; Ting, A. Nonlinear interaction of intense laser pulses in plasmas. *Phys. Rev. A* **1990**, *41*, 4463–4469. [CrossRef]
21. Tomassini, P.; Massimo, F.; Labate, L.; Gizzi, L.A. Accurate electron beam phase-space theory for ionization-injection schemes driven by laser pulses. *High Power Laser Sci. Eng.* **2022**, *10*, e15. [CrossRef]
22. Schroeder, C.; Vay, J.L.; Esarey, E.; Bulanov, S.; Benedetti, C.; Yu, L.L.; Chen, M.; Geddes, C.; Leemans, W. Thermal emittance from ionization-induced trapping in plasma accelerators. *Phys. Rev. Spec. Top. Accel. Beams* **2014**, *17*, 101301. [CrossRef]
23. Pukhov, A.; Gordienko, S.; Kiselev, S.; Kostyukov, I. The bubble regime of laser–plasma acceleration: Monoenergetic electrons and the scalability. *Plasma Phys. Control. Fusion* **2004**, *46*, B179. [CrossRef]
24. Lehe, R.; Kirchen, M.; Andriyash, I.A.; Godfrey, B.B.; Vay, J.L. A spectral, quasi-cylindrical and dispersion-free Particle-In-Cell algorithm. *Comput. Phys. Commun.* **2016**, *203*, 66–82. [CrossRef]